

doi.org/10.1002/elan.202200349

A Comparative Study of Voltammetric vs Impedimetric Immunosensor for Rapid SARS-CoV-2 Detection at the Point-of-care

Cristina Tortolini,^[a] Antonio Angeloni,^[a] and Riccarda Antiochia*^[b]

Abstract: Here, a novel biosensing platform for the detection of SARS-CoV-2 usable both at voltammetric and impedimetric mode is reported. The platform was constructed on a multi-walled carbon nanotubes (MWCNTs) screen-printed electrode (SPE) functionalized by methylene blue (MB), antibodies against SARS-CoV-2 spike protein (SP), a bioactive layer of chitosan

(CS) and protein A (PrA). The voltammetric sensor showed superior performances both in phosphate buffer solution (PBS) and spiked-saliva samples, with LOD values of 5.0 ± 0.1 and 30 ± 2.1 ng/mL, compared to 20 ± 1.8 and 50 ± 2.5 ng/mL for the impedimetric sensor. Moreover, the voltammetric immunosensor was tested in real saliva, showing promising results.

Keywords: Immunosensor · SARS-CoV-2 · voltammetric biosensor · impedimetric biosensor · POC diagnostics

1 Introduction

The emergence of the new viral disease COVID-19 highlights the need for fast methods to detect and identify the target SARS-CoV-2 virus at scale [1]. The SARS-CoV-2 belongs to the big family of coronaviruses, identified as human pathogens in the 1960s [2]. There are currently seven coronaviruses known to infect humans. Three of them emerged more recently and cause severe, even fatal disease: SARS-CoV [3], MERS-CoV, [4,5], and SARS-CoV-2, which emerged in Wuhan, China in late 2019, and then spread rapidly across the globe affecting billions of people worldwide [6,7].

It is well known that coronaviruses are transmitted from person to person via respiratory droplets, and /or aerosols generated when coughing and speaking, and that also asymptomatic individuals can transmit the disease [8,9]. Although the COVID-19 vaccination program reached encouraging results, a successful vaccination of the global population is a crucial issue to be achieved and, at the same time, new variants are rapidly emerging. Therefore, identification of infected individuals based on reliable diagnostic tests is still the only way to contain the spread of the virus. In this context, diagnostic tests based on highly sensitive, simple, fast, low-cost and easy-to-use detection methods for early diagnosis of COVID-19 continue to be urgently needed [10–15].

Several diagnostic methods of COVID-19 have been reported, including real-time polymerase chain reaction (RT-PCR) [16–18], lateral flow immunoassay (LFIA) [19], enzyme-linked immunosorbent assay (ELISA) [20] and computed tomography (CT) imaging [21]. RT-PCR remains the “gold standard” diagnostic method for COVID-19. However, it has the drawback to be time-consuming and expensive, requiring both specialized personnel and laboratories, and with a high false-negative

ratio [22]. LFIA and ELISA based methods are moderately fast and less expensive, despite having lower sensitivity and still showing false-negative results [23]. CT imaging shows better false-negative rates but suffers from low specificity, as the obtained imaging may overlap with different viral pneumonia. Moreover, it is not suitable for point-of-care (POC) testing and early diagnosis [24].

Electrochemical biosensing technologies represent an interesting compromise between high sensitivity, specificity, low cost, simplicity, rapidity and possibility of on-site COVID-19 detection [25–30]. Up to now, several biosensors have been developed for SARS-CoV-2 detection [31–39], some of them still requiring an RNA extraction step before detection and/or expensive equipment and trained personnel [33,40–43]. Most of them are either voltammetric- or impedimetric-mode based, but no explanation regarding the detection mode utilized is reported.


In the present paper, we describe the development of a dual-mode disposable electrochemical immunosensor for SARS-CoV-2 detection based on either differential


[a] C. Tortolini, A. Angeloni

Department of Experimental Medicine, University of Rome “La Sapienza”, Viale Regina Elena 324, 00166 Rome, Italy

[b] R. Antiochia

Department of Chemistry and Drug Technologies, University of Rome “La Sapienza”, P.le Aldo Moro 5, 00185, Rome, Italy
E-mail: riccarda.antiochia@uniroma1.it

 Supporting information for this article is available on the WWW under <https://doi.org/10.1002/elan.202200349>

 © 2022 The Authors. Electroanalysis published by Wiley-VCH GmbH. This is an open access article under the terms of the Creative Commons Attribution Non-Commercial NoDerivs License, which permits use and distribution in any medium, provided the original work is properly cited, the use is non-commercial and no modifications or adaptations are made.

pulse voltammetry (DPV) or electrochemical impedance spectroscopy (EIS) signals. The selective interaction and successively binding between the SARS-CoV-2 antibody and spike protein, both immobilized on the surface of a MWCNTs electrochemical platform firstly functionalized with MB, CS and PrA, produces a sudden change in the redox probe electron transfer kinetics, detectable by either a decrease of the voltammetric current or an increase of the charge-transfer resistance (R_{CT}). The electrochemical performances of the voltammetric and impedimetric immunosensors were investigated in PBS, spiked and real saliva samples. The detection methods were compared, highlighting the advantaged and drawbacks of each of them. Finally, the voltammetric-mode immunosensor was tested with a portable potentiostat enabling wireless smartphone connection and an easy POC signal readout.

2 Materials and Methods

2.1 Chemicals and Reagents

Methylene blue (MB, dye content, $\geq 82\%$), chitosan (CS, low molecular weight: 50,000–190,000 g mol^{-1}), protein-A (PrA) from *Staphylococcus aureus*, sodium monobasic phosphate (Na_2HPO_4), sodium dibasic phosphate NaH_2PO_4 , potassium chloride (KCl), potassium ferricyanide (III) ($\text{K}_3[\text{Fe}(\text{CN})_6]$), potassium ferrocyanide (II) ($\text{K}_4[\text{Fe}(\text{CN})_6]$), bovine serum albumin (BSA) were purchased from Sigma-Aldrich (Buchs, Switzerland). SARS-CoV-2 Spike Antibody (anti-SP, Rabbit MAb), SARS-CoV-2 Spike S1-His Recombinant Protein (SP, Cat. Number 40591-V08H, molecular mass 76.5 kDa), MERS-CoV spike/S1 protein (S1 Subunit, aa 1–725), Influenza A H1N1 (Hemagglutinin/HA Protein) and Influenza B (Neuroaminidase/NA) were furnished by Sino Biological Europe GmbH (Eschborn, Germany). All solutions were prepared in phosphate buffer 10 mM, KCl 0.1 M, pH 7.4 (PBS). High purity deionized water (resistance: 18.2 $\text{M}\Omega\text{cm}$ at 25 °C; $\text{TOC} < 10 \mu\text{g L}^{-1}$) obtained from Millipore (Molsheim, France) has been used throughout experiments.

The absence and presence of SARS-CoV-2 in clinical saliva samples were performed by Hightop SARS-CoV-2 Antigen Rapid Test (Qingdao Hightop Biotech Co., Ltd, Qingdao, Shandong, China).

2.2 Instrumentation and Electrodes

Electrochemical measurements for platform characterization, optimization studies (paragraphs 3.2, 3.3) and immunosensor analytical performances studies were carried out in a 10 mL thermostated glass cell (model 6.1415.150, Metrohm, (Herisau, Switzerland) with a conventional three-electrode configuration consisting of an $\text{Ag}/\text{AgCl}/\text{KCl}_{\text{sat}}$ (198 mV vs. NHE), as reference electrode (cat. 6.0726.100, Metrohm, Herisau, Switzerland), a glassy carbon rod as counter electrode (cat. 6.1248.040, Met-

rohm, Herisau, Switzerland) and a MWCNTs-COOH functionalized screen-printed electrode (110-CNT, Metrohm, Herisau, Switzerland), as working electrode (MWCNTs SPE), using an Autolab Potentiostat/Galvanostat (Eco Chemie, Netherlands).

Scanning electron microscopy (SEM) and energy-dispersive X-ray spectroscopy analysis (EDX) measurements were performed with High-Resolution Field Emission Scanning Electron Microscopy (HR FESEM, Zeiss Auriga Microscopy, Jena, Germany).

For the smartphone-based sensing device experiments, a Sensit/SMART portable potentiostat (PalmSens, Houten, The Netherlands) was used and directly connected to a smartphone for POC signal reading.

2.3 Electrochemical Measurements

All the electrochemical measurements were recorded using freshly prepared Zobell's solution (5 mM solution of ferrocyanide/ferricyanide $[\text{Fe}(\text{CN})_6]^{3-/4-}$ 1.1 ratio, in PBS pH = 7.4 [44]).

DPV measurements were recorded by scanning from -0.2 to 0.6 V, amplitude 20 mV and step potential 5 mV. Base-line corrections were done for all DPV data using the NOVA software. Electrochemical measurements were reported as $(I-I^0)/I$, where I^0 is the current of the blank sensor and I is the current after drop-casting of the SP antigen solutions on the SARS-CoV-2 immunosensor platform.

EIS experiments were carried out at equilibrium potential called open circuit potential (OCP) without bias voltage in the frequency range of 0.1 – 10^5 Hz (MWCNTs SPE electrodes), using an ac signal of 10 mV amplitude at the formal potential of the redox probe (0.22 V vs Ag/AgCl).

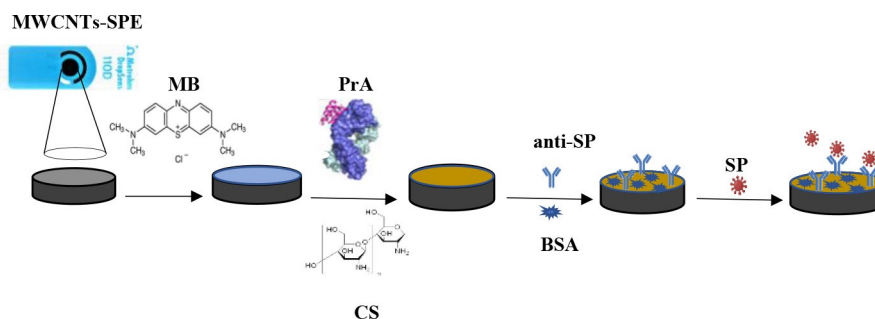
Single-drop analysis on the surface of anti-SP/BSA/PrA/MB/MWCNTs SPE sensor using DPV and EIS techniques has been performed as follows: i) separate solutions of different SP concentrations in PBS and in saliva were prepared; ii) for single analysis, a 50 μL drop was pipetted on to the surface of the sensor; iii) immediately after applying the drop, a measurement was carried out. After each measurement, the surface of the SPE was rinsed with distilled H_2O and successively dried under a stream of N_2 gas. After this cleaning procedure, another drop was pipetted, and a new measurement was performed.

All experiments have been designed with three replicates ($n = 3$).

2.4 Immunosensor Modification

The sequence of the modification steps employed in the SARS-CoV-2 immunosensor development is reported in Scheme 1.

Firstly, MWCNTs SPEs were modified by electropolymerization of methylene blue (MB, 0.1 mM in PBS) by cyclic voltammetry (CV), scanning the potential



Scheme 1. Sequence of surface modification steps for the anti-SP/PrA/CS/MB/MWCNTs-SPE immunosensor platform preparation.

between $-1.0 \div 1.0$ V, at $v=100$ mVs $^{-1}$ for 20 scans. Then, a CS layer ($4 \mu\text{L}$, 0.5 mg mL $^{-1}$ in 1% (w/v) acetic acid) was drop-cast on the electrode surface and incubated for 30 min at room temperature (RT). After, $4 \mu\text{L}$ of PrA from *S. aureus* ($4 \mu\text{L}$, $45 \mu\text{g mL}^{-1}$ in PBS buffer) was dropped on the MB/CS electrode surface for 50 min at RT. Immobilization of anti-SP was achieved by drop-casting the antibody ($3 \mu\text{L}$, $20 \mu\text{g mL}^{-1}$) onto the PrA/CS/MB modified electrode surface and let to bind for 30 min at RT. Finally, the antibody modified electrode was incubated for 30 min with BSA solution ($2 \mu\text{L}$, 0.25% w/v), used as blocking agent to avoid non-specific interactions. At the end of each modification step, the modified electrode was washed with distilled water. The anti-SP/PrA/CS/MB/MWCNTs-SPE immunosensor was stored at $2-8^\circ\text{C}$ before use.

2.5 Selectivity Experiments

Selectivity studies of the voltammetric immunosensor were performed with MERS-CoV, Influenza A, Influenza B antigens at a concentration of $10 \mu\text{g/mL}$ and S-protein at a concentration of $1 \mu\text{g/mL}$. After 15 minutes incubation time of each virus on the anti-SP/BSA/PrA/CS/MB/MWCNTs-SPE platform, DPV measurements were conducted in triplicate.

2.6 Clinical Samples Testing

Saliva samples were collected from healthy donors (attested by negative result by RT-PCR) and from patients with a wide range of symptoms (positive result by RT-PCR) with the express consent to such collection of the person from whom this material was taken, according to the current legislation. The samples were heated at 56°C for 1 h for viral inactivation according to the appropriate biosafety procedure (2020 CDC COVID-19 test protocol for details on specimen collection). Successively, the samples of raw saliva ($50 \mu\text{L}$) were directly used by drop-casting on the electrode surface and left for 15 min incubation time. They were used immediately or kept at -80°C until further use.

3 Results and Discussion

3.1 FESEM and EDX Characterization of the Immunosensor

The morphological structures of the modified SPEs were analyzed by field emission scanning electron microscopy (FESEM) and energy-dispersive X-ray spectroscopy analysis (EDX). The FESEM images of bare MWCNTs-SPE displayed the surface consisting of a uniform layer of carbon nanotubes (Figure 1, panel A). The EDX spectrum confirmed the presence of only carbon and oxygen elements. The atomic percentage of C and O, calculated from the quantification of the peaks, gave a value of about 96 and 3%, respectively. The presence of Cl element is probably due to possible impurities present in the commercial MWCNTs-SPEs (Figure 1, panel B). After the MB electropolymerization, a uniformly distributed MB layer resulted clearly visible on the nano-modified electrode surface (Figure 1, panel C). Unlike pristine MWCNTs-SPE, S and N additional peaks appeared in the EDX spectrum, due to proper MB-electro-adsorbed functionalization, with an atomic percentage, calculated from the quantification of the peaks, of about 0.3 and 0.1%, respectively. Although these values are very small, probably due to the low concentration of the polymer solution employed (0.1 mM), they still reflect the elemental composition of the MB molecule (Figure 1, panel D). Finally, the FESEM image of the anti-SP/PrA/CS/MB/MWCNTs-SPE immunosensor platform is reported (Figure 1, panel E). A macro-structured surface is clearly visible, confirming that the large antibody, protein A, chitosan and BSA biomolecules well cover the electrode surface. Moreover, the EDX mapping of the latter platform shows the increased amount of the N element, due to the presence of chitosan and protein molecules, and of several heteroatoms, such as Na, P and K, confirming the successful immobilization of both protein A and antibody on the nanostructured surface (Figure 1, panel F).

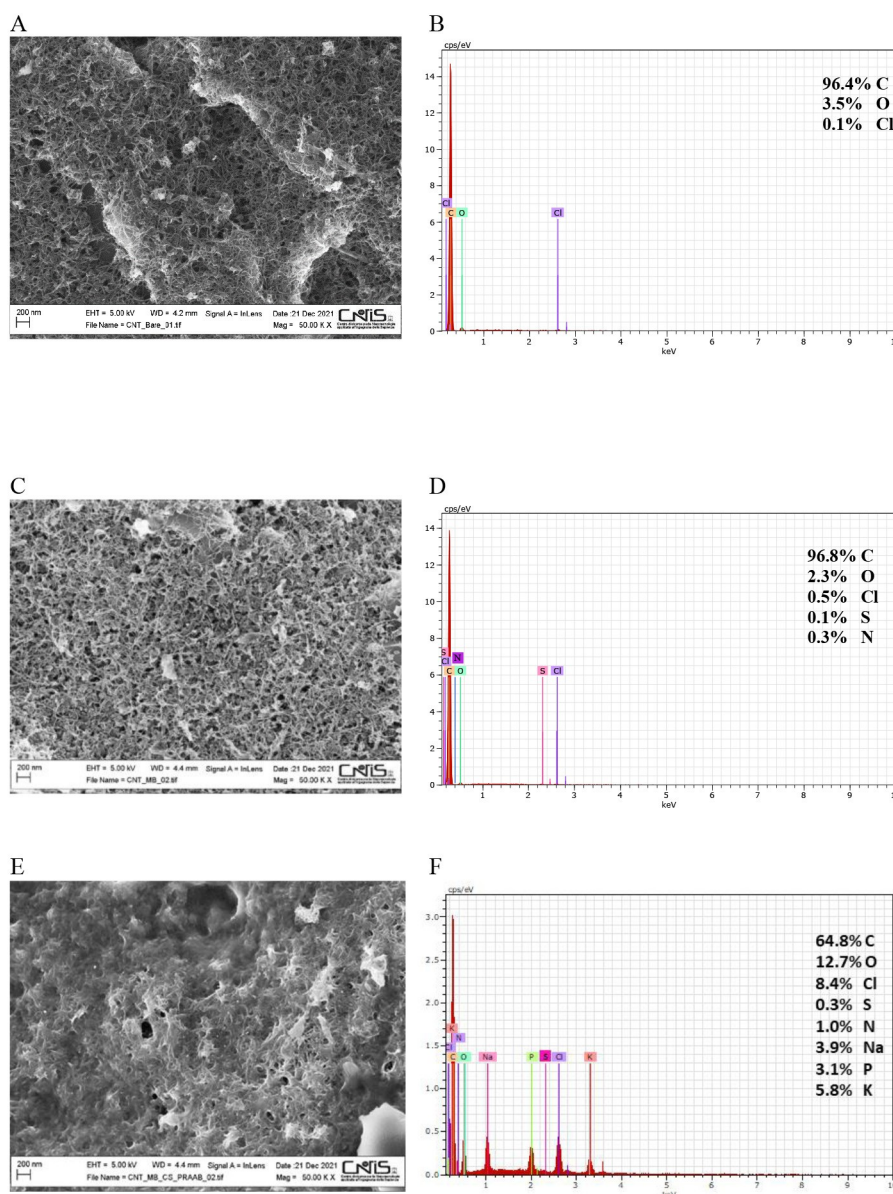


Fig. 1. SEM images and EDX spectra for MWCNTs-SPE (panel A and B), MB/MWCNTs-SPE (panel C and D) and anti-SP/BSA/PrA/CS/MB/MWCNTs-SPE (panel E and F). Experimental conditions: magnification 50,000 X; voltage 10 kV.

3.2 Electrochemical Characterization of the Immunosensor

Differential pulse voltammetry (DPV) and electrochemical impedance spectroscopy (EIS) techniques were performed to investigate the MWCNTs-SPE electrode behavior after each surface modification step (Figure 3A, B).

The DPV curves relative to the bare and sequentially modified electrodes are shown in Figure 2, panel A. After MB electropolymerization, a three-times current increase (blue curve), compared to bare electrode (black curve), is observed, according to the excellent electroactive properties of MB. Furthermore, the immobilization of CS

biolayer and PrA causes a further increase of peak current (red curve), indicating the enhanced electron transfer, thanks to the excellent electroconductivity of the chitosan biopolymer. The DPV curve observed in absence of PrA does not show any significant difference with the red curve (curve not shown), attesting that the bioactive layer of PrA does not show electroconductive properties under the conditions used, but only a functional role for the sensor design and biorecognition activity. The PrA moieties seem to facilitate the proper orientation and exposure of the antibody sites to epitopes [45].

The further immobilization of antibody and BSA, used as blocking agent of the non-binding sites of the sensor surface, causes a visible reduction of the peak

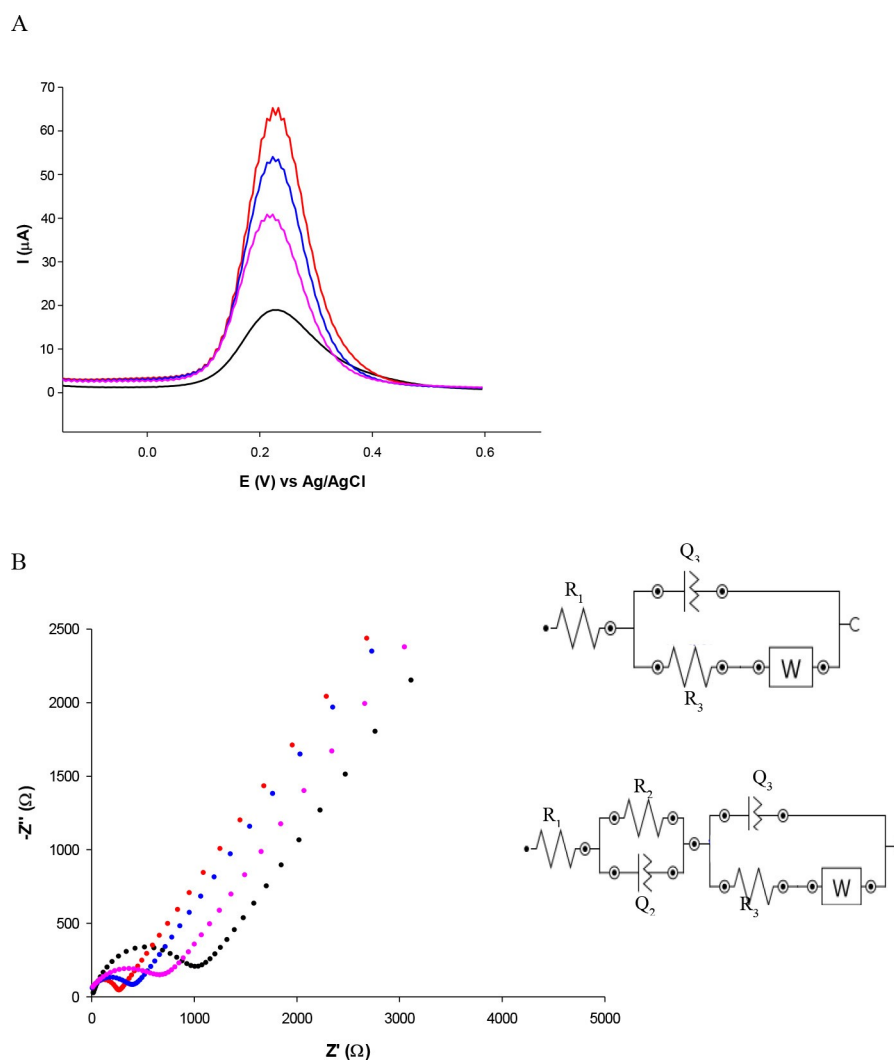


Fig. 2. A) DPVs of bare (black), MB (blue), PrA/Cs/MB (red), anti-SP/BSA/PrA/Cs/MB/MWCNTs-SPE (pink) measured in Zobell's solution. B) Nyquist plots of bare (black), MB (blue), MB/CS/PrA (red), MB/CS/PrA/anti-SP/BSA (pink) MWCNTs-SPE measured in Zobell's solution. Inset: Randles (1) and Randles modified (2) equivalent circuits.

current (pink curve), which indicates that the electron transfer through the electrode surface is now hampered, probably due to the insulating nature of both antibody and BSA molecules, with a consequent decrease of the effective electrode surface area.

EIS experiments were successively used to confirm each modification step of the working electrode.

Figure 2, panel B, displays the EIS spectra for the unmodified and modified electrode surface platforms performed in the Zobell's solution. The semicircle of the Nyquist plot represents the charge transfer resistance (R_{ct}) of the system, which is strictly related to very small changes at the interface electrode/electrolyte solution. After the immobilization of a bio-molecule over the electrode surface, the electron transfer rate between the redox probe and the electrochemical double layer retarded, thus causing an increase in R_{ct} value for the redox probe to access the electrochemical double layer.

A decrease of the semicircle is initially observed after the MB electropolymerization step (blue curve) and a further decrease after the CS/PrA immobilization step (red curve), proving that both MB and CS films increase the conductivity at the interface, thanks to their excellent electroconductive properties. An opposite trend is observed after the immobilization of the anti-SP/BSA on the modified electrode, showing a large increase of the semicircle diameter. The covalent binding of antibody and BSA makes electrode surface more insulating, causing an electron transfer hindrance and a consequent increase of the R_{ct} value.

The impedance spectra were fitted by two different equivalent circuits (inset Figure 2, panel B), depending on the surface modification. For bare and MB modified electrodes, a simple Randles circuit [R(Q[RW])] was successfully utilized (circuit 1). For further modified electrodes, a different equivalent circuit, comprising two semi-arc regions and a Warburg element, was proposed

[R(RQ)(Q[RW])] (circuit 2). The goodness of the fitting was confirmed by the χ^2 value obtained for each step, as reported in Figure S1, where it is clearly visible the agreement between the EIS experimental data (green circles) and the fitting (blue line) for the anti-SP/BSA/PrA/CS/MB/MWCNTs-SPE platform. As shown in Table 1, the R_3 value decreased from 974 Ω to 264 Ω after the MB modification of the bare electrode, attesting about 73 % decrease, calculated according to the following equation:

$$\Delta R_{ct} = (R_{3b} - R_{3m})/R_{3b} \times 100\%$$

where R_{3b} is the R_{ct} for the bare electrode and R_{3m} is the R_{ct} for the modified electrode, respectively.

The further addition of the CS layer and PrA showed a further reduction of the R_3 value to 85 %. Finally, when the antibody and BSA were deposited onto the CS/MB/MWCNTs-SPE, the R_{ct} values expressed as R_2 and R_3 increased, as active sites decreased.

The results of EIS perfectly aligned with those obtained with SEM, EDX and DPV experiments, confirming the composition of the electrodes' surface after each modification step.

3.3 Optimization Studies

As the developed immunosensor is based on affinity interactions between S-protein and the specific antibody, the anti-SP concentration and its binding time on the

modified electrode surface were investigated by DPV technique. The optimal antibody concentration resulted to be 20 $\mu\text{g/mL}$ with a binding time of 30 minutes (Figure S2, panel A and B).

DPV experiments were also used to investigate the optimum incubation time of SP for different time periods between 5 and 30 minutes. The maximum current response was observed at an incubation time of 15 min (Figure S2, panel C), demonstrating the reaching of the electrode surface saturation for the optimized antibody concentration.

The optimum values obtained were used for further experiments.

3.4 Response of the Immunosensor to SARS-CoV-2 Spike Protein

The response of the anti-SP/BSA/PrA/CS/MB/MWCNTs-SPE immunosensor against SARS-CoV-2 spike protein has been evaluated with DPV and EIS electrochemical techniques.

3.4.1 Voltammetric Immunosensor

The DPV curves and the relative calibration plot of the anti-SP/PrA/CS/MB/MWCNTs-SPE immunosensor obtained with different concentrations of SARS-CoV-2 spike antigen in PBS using $[\text{Fe}(\text{CN})_6]^{3-/4-}$ as redox probe, are reported in Figure 3 (panel A and B). When the antigen is specifically attached to the antibody, the probe

Table 1. Comparison of R_{ct} values of bare and modified MWCNTs-SPE after each modification step.

Modification step	MWCNTs-SPE					
	R_3 (Ω/cm^2)	R_2 (Ω/cm^2)	$Q_{3 \times 10}^{-6}$ (Ωs^N)	$Q_{2 \times 10}^{-6}$ (Ωs^N)	W ($\mu\Omega\text{s}^{1/2}$)	$\chi^2 \times 10^{-3}$
Bare*	974	–	1.83	–	415	0.2
MB*	264	–	0.11	–	366	0.3
MB/CS/PrA**	147	233	0.020	0.59	376	2.9
MB/CS/PrA/anti-SP/BSA**	150	486	0.016	0.82	363	3.4

* Data obtained by using circuit 1; ** data obtained by using circuit 2.

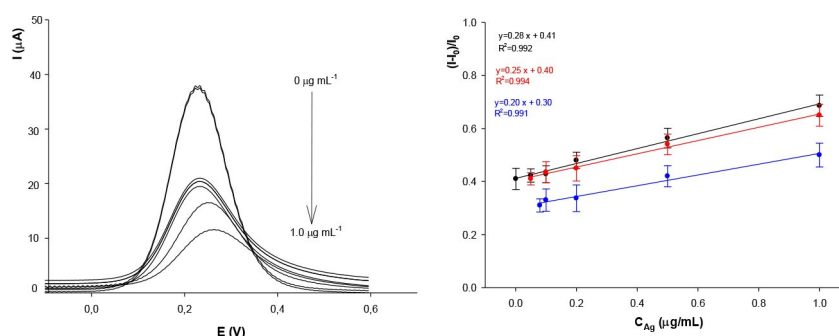


Fig. 3. (A) DPV peak currents of anti-SP/BSA/PrA/CS/MB/MWCNTs-SPE immunosensor for different SP concentrations (0.01, 0.05, 0.1, 0.2, 0.5, 1.0 $\mu\text{g/mL}$); (B) Calibration plot for the normalized $(I-I_0)/I_0$ ratio, $n=3$, in PBS (black curve), in spiked-saliva samples (red curve) and in spiked-saliva by using the Sensit/SMART (blue curve). Experimental conditions: 5 mM $[\text{Fe}(\text{CN})_6]^{3-/4-}$ in 0.1 M PBS, pH = 7.4; 3 μL anti-SP 20 $\mu\text{g/mL}$ and 30 min antibody binding time.

electron-transfer is hindered, as observed by the progressive peak current decrease. A linear plot according to the DPV measurements expressed as $I-I_0/I_0$ ratio, where I_0 is the peak current value of the biodevice without antigen and I is the peak current value of the modified voltammetric sensor, measured with different antigen concentrations, was obtained. The immunosensor demonstrated a linear dynamic response to SARS-CoV-2 spike protein between 0.01 $\mu\text{g/mL}$ and 1.00 $\mu\text{g/mL}$ (Figure 3, panel B, black curve). The linear regression equation obtained by fitting the data point was $y=0.28x+0.41$, with a correlation coefficient of 0.990. The limits of detection (LOD) and quantification (LOQ) have been calculated as 5.0 ± 0.1 ng/mL and 15 ± 0.3 ng/mL, respectively, according to the $3\sigma/m$ formula, where σ represents the standard deviation of the blank and m indicated the slope of the calibration plot.

The proposed immunosensor was successively tested in SARS-CoV-2 spike protein spiked-saliva samples. From the DPV curves (not shown), the calibration plot has been constructed at a concentration ranging from 0.05 $\mu\text{g/mL}$ to 1.00 $\mu\text{g/mL}$, with LOD and LOQ values calculated as 30 ± 2.1 ng/mL and 100 ± 4.7 ng/mL, respectively (Figure 3, panel B, red curve). A slightly shorter linear range and higher LOD and LOQ values have been observed in spiked saliva compared to PBS solution, indicating that potential interferents present in the complex saliva matrix, such as proteins and other biomolecules, may cause biofouling of the electrode surface, thus affecting the current signal.

3.4.2 Impedimetric Immunosensor

The EIS spectra obtained after the addition of different concentrations of SARS-CoV-2 spike antigen diluted in PBS using $[\text{Fe}(\text{CN})_6]^{3-/4-}$ as redox probe are shown as

Nyquist plots and reported in Figure 4, panel A. At high frequencies, the impedance clearly increases at increasing SP concentrations, thus demonstrating the interaction of the SARS-CoV-2 SP with the biofunctionalized electrode surface. The sequential increase of the diameter of the semi-circles of the Nyquist plot, representing the charge transfer resistance, is correlated to the stepwise steric hindrance increase due to the antigen binding. The relative calibration plot corresponding to the variation of $R_{ct}-R_{ct0}/R_{ct0}$ % vs. SP concentration in PBS solution, is shown in Figure 4, panel B (black curve). The impedimetric immunosensor presents a linear dynamic range between 0.05 $\mu\text{g/mL}$ and 1.00 $\mu\text{g/mL}$ with a LOD and LOQ value of 20 ± 1.8 ng/mL and 55 ± 2.6 ng/mL, respectively.

As for the voltammetric immunosensor, the proposed impedimetric immunosensor has been tested in saliva samples spiked with SARS-CoV-2 SP, and the corresponding calibration plot is reported in Figure 4, panel B (red curve). A slightly shorter linear range from 0.1 to 1.0 $\mu\text{g/mL}$ was obtained, with LOD and LOQ values of 50 ± 2.5 and 140 ± 5.3 ng/mL, respectively. Once again, higher LODs and LOQs are consistent with the more complex saliva matrix, which implies a decrease of the sensor sensitivity.

3.5 Selectivity Studies

Cross-reactivity studies were performed by using 4 μL of MERS-CoV, Influenza A, Influenza B at a concentration of 10 $\mu\text{g/mL}$ and SP at a concentration of 1 $\mu\text{g/mL}$. After 15 minutes incubation time of each virus on the anti-SP/BSA/PrA/CS/MB/MWCNTs-SPE platform, a significant current decrease has been observed after the interaction with SP, while very small decreases were registered in the DPV curves for the other virus tested, although they are

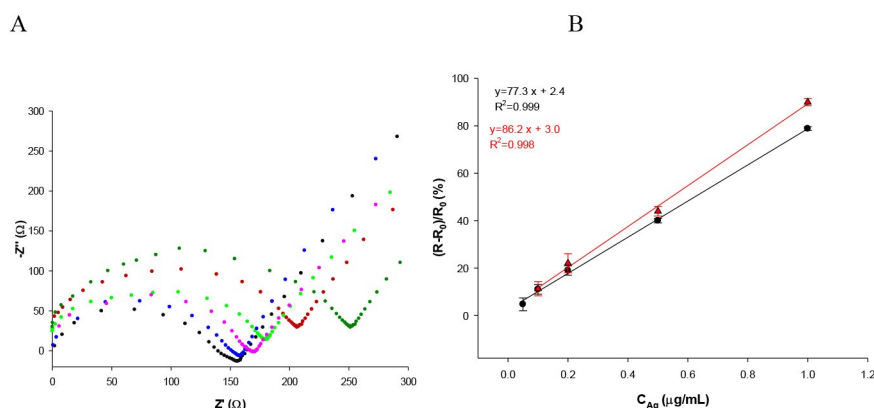


Fig. 4. (A) Nyquist plots of faradaic measurements of anti-SP/BSA/PrA/Cs/MB/MWCNTs-SPE immunosensor at different SARS-CoV-2 SP concentrations (0.05, 0.1, 0.2, 0.5, 1.0 $\mu\text{g/mL}$); (B) Corresponding linear calibration plot for the normalized $(R-R_0)/R_0$ ratio, $n=3$ in PBS (black curve) and in spiked-saliva samples (red curve). Experimental conditions: 5 mM $[\text{Fe}(\text{CN})_6]^{3-/4-}$ in 0.1 M PBS pH=7.4; 3 μL anti-SP 20 $\mu\text{g/mL}$ and 30 min antibody binding time

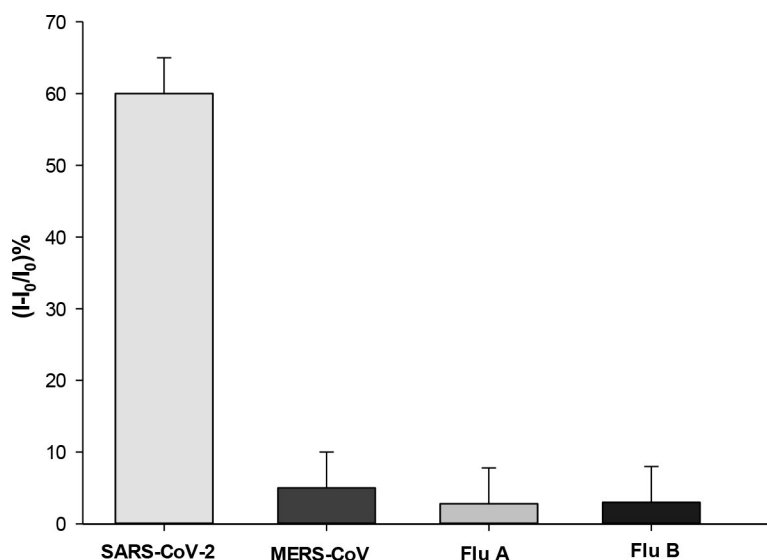


Fig. 5. Histogram showing selective detection of anti-SP vs. different virus proteins. Experimental conditions: 3 μL of 20 $\mu\text{g}/\text{mL}$ of anti-SP, 30 min immobilization time, on the working electrode of BSA/PrA/CS/MB/MWCNTs-SPE. Then 4 μL of 1 $\mu\text{g}/\text{mL}$ SARS-CoV-2 and 10 $\mu\text{g}/\text{mL}$ of MERS-CoV-2, Flu A, Flu B, respectively, for 45 min incubation time on anti-SP/BSA/PrA/CS/MB/MWCNTs-SPE. Each measurement was performed dropping 50 μL of Zobell's solution on anti-SP/BSA/PrA/CS/MB/MWCNTs-SPE ($n=3$).

used at 10 times higher concentration. These results clearly indicate no cross-reactivity event against the virus tested (Figure 5).

3.6 Reproducibility, Repeatability, Stability Studies and Response Time

To investigate the reproducibility of the voltammetric immunosensor, five modified electrodes were used to detect 0.1 $\mu\text{g}/\text{mL}$ of SP. The RSD obtained was 2.5%. The repeatability was calculated by using the same electrode platform for five repeated measurement of 0.1 $\mu\text{g}/\text{mL}$ of SP, and the RSD obtained was 1.6%, confirming an excellent reproducibility and repeatability of the proposed immunosensor.

In order to check the long-term stability of the proposed platform, the life-time of the voltammetric sensor was evaluated by measuring the peak current every day over a period of 14 days, after the addition of a 0.1 $\mu\text{g}/\text{mL}$ of SP ($n=3$). After use, the sensor was stored in PBS at 4°C. The sensor showed a slightly decreasing trend of the current, maintaining 90% of its initial response after two weeks, probably thanks to the synergistic effect of electrode surface nano-structuration and functionalization with CS and PrA, which facilitates and amplifies the efficient binding of the antibodies and the subsequent durable immune complex formation with the target antigens (Figure S3). The results confirm the high stability of the sensor platform.

As for the immunosensor response time, the voltammetric detection allowed a shorter response time of 2 minutes, compared to 10 minutes for the impedimetric mode-based sensor.

3.7 Clinical Sample Analysis

To assess the efficiency of the voltammetric immunosensor using clinical samples, saliva samples of 20 healthy individuals and 10 infected individuals 5 days after symptoms onset, identified by RT-PCR analysis, were tested using the proposed voltammetric immunosensor and a commercially available rapid antigen test (RAT). It was decided to set 2 μA (ΔI_p) current decrease as threshold for positive samples. We used saliva samples collected from individuals after drinking a glass of water, in order to match the requirement of a POC device.

As reported in Table 2, we observed an agreement with RT-PCR in 9/10 samples for positive results and 18/20 samples for negative results (not shown), which is a very satisfactory result, indicating a 91.6% sensitivity and

Table 2. Results obtained from RT-PCR, anti-SP/BSA/PrA/CS/MB/MWCNTs-SPE voltammetric immunosensor and rapid antigen test (RAT) for COVID-19 positive patients on saliva samples.

Sample	RT-PCR (nasopharyngeal swabs)	Immunosensor (saliva)	RAT (nasopharyngeal swabs)
Patient#1	+	+	+
Patient#2	+	+	+
Patient#3	+	+	+
Patient#4	+	-	-
Patient#5	+	+	+
Patient#6	+	+	+
Patient#7	+	+	-
Patient#8	+	+	+
Patient#9	+	+	+
Patient#10	+	+	-

90.0% specificity for positive and negative samples. By comparing the accuracy of the proposed immunosensor and rapid antigen tests in positive samples, the developed immunosensor responded more accurately, achieving 90% accuracy, compared to 70% accuracy of the RAT, used a comparison. It is interesting to note that the proposed immunosensor seems to reduce false-negative results, compared to the commercially available RATs.

Finally, it is interesting to note that by comparing the two proposed immunosensors to other voltammetric and impedimetric COVID-19 biosensors recently reported in literature, the impedimetric immunosensor shows superior performances [46–49], while the voltammetric immunosensor is within acceptable limits [32–34, 50–54]. However, it must be highlighted that most voltammetric immunosensors reported in literature are DNA-based sensors, which detect the viral genes after a viral RNA extraction step, followed, in some cases, by an amplification step [40, 55]. Otherwise, the proposed immunosensor offers the advantages of direct and quick detection of SARS-CoV-2 without any further treatment of the specimen.

4 Conclusions

Here we report a comparative study between voltammetric and impedimetric SARS-CoV-2 immunosensors, based on the same anti-SP/BSA/PrA/CS/MB/MWCNTs/SPE platform. Both sensors showed promising results and potential for detection of SARS-CoV-2 SP in PBS and spiked-saliva samples with good sensitivity. Our study suggests some advantages of the voltammetric sensor in terms of wider linear range, lower detection limit, shorter response-time and lower costs. Stability, operational simplicity, reproducibility and repeatability are comparable for both immunosensors, being related to the electrochemical platform characteristics and totally independent on the sensing detection mode.

Moreover, the voltammetric immunosensor showed excellent selectivity and accuracy for the detection of COVID-19 in real saliva samples and a perfect agreement with RT-PCR results, demonstrating that saliva represents a suitable and undervalued resource for COVID-19 testing. Further, the proposed voltammetric sensor showed satisfactory results when used with a portable potentiostat directly connected to a smartphone for POC signal reading.

For these reasons, the proposed immunosensor platform with voltammetric detection would be suitable to implement POC testing for COVID-19 telemedicine care and remote monitoring.

Acknowledgements

This work was supported by Italian Ministry of Education, Universities and Research, Progetto di Ateneo2019, No. RG11916B798EED5E.

Open Access Funding provided by Università degli Studi di Roma La Sapienza within the CRUI-CARE Agreement.

Data Availability Statement

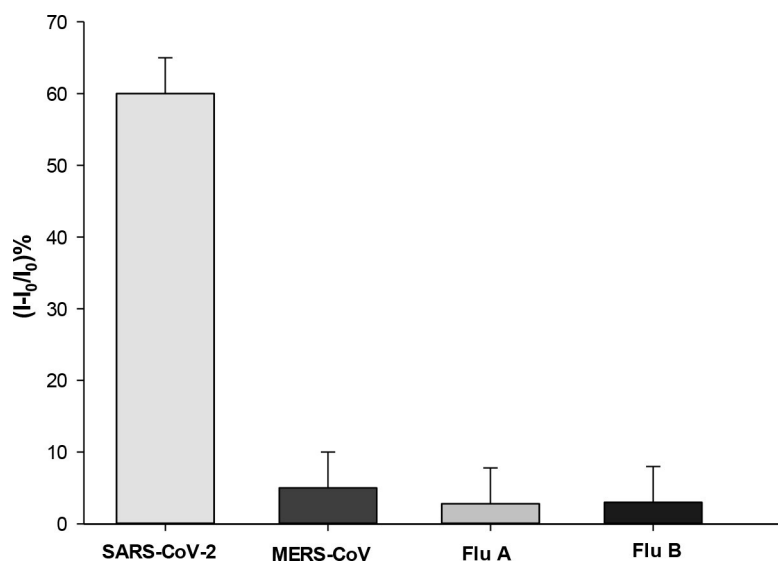
This is an open access article under the terms of the Creative Commons Attribution-NonCommercial-NoDerivs License, which permits use and distribution in any medium, provided the original work is properly cited, the use is non-commercial and no modifications or adaptations are made.

References

- [1] WHO, World Health Organization, 2020. Coronavirus disease 2019 (COVID-19): situation report, 40. World Health Organization, pp. 1–7.
- [2] J. S. M. Peiris, 2012. Coronaviruses, In: *Medical microbiology* (8th edition), Churchill Livingstone, pp. 587–593.
- [3] J. S. M. Peiris, Y. Guan, K. Y. Yuen, *Nat. Med.* **2004**, *10* (12Suppl), 88–97.
- [4] A. Assiri, J. A. Al-Tawfiq, A. A. Al-Rabeeh, F. A. Al-Rabiah, S. Al-Hajjar, A. Al-Barrak, H. Flemban, W. N. Al-Nassir, H. H. Balkhy, R. F. Al-Hakeem, H. Q. Makhdoom, A. I. ZumLa, Z. A. Memish, *Lancet Infect. Dis.* **2013**, *13* (9), 752–761.
- [5] M. Xie, Q. Chen, *IJID* **2020**, *94*, 119–124.
- [6] C. C. Lai, T. P. Shin, W. C. Ko, H. J. Tang, R. P. Hsueh, *Int. J. Antimicrob. Agents* **2020**, *55* (3), 105924.
- [7] N. C. Peeri, N. Shrestha, M. S. Rahman, R. Zaki, Z. Tan, S. Bibi, M. Baghbanzadeh, N. Aghamohammadi, W. Zhang, U. Haque, *Int. J. Epidemiol.* **2020**, *1*, 1–10.
- [8] M. Fani, A. Teimoori, S. Ghafari, *Future Virol.* **2020**, *15* (5), 317–323.
- [9] H. Nishiura, T. Kobayashi, T. Miyama, A. Suzuki, S. Jung, K. Hayashi, R. Kinoshita, Y. Yang, B. Yuan, A. R. Akhmetzhanov, N. M. Linton, *IJID* **2020**, *94*, 154–155.
- [10] B. Giri, S. Pandey, R. Shrestha, K. Pokharel, F. S. Ligler, B. B. Neupane, *Anal. Bioanal. Chem.* **2020**, *413* (1), 35–48.
- [11] E. Sheikhzadeh, S. Eissa, A. Ismail, M. Zourob, *Talanta* **2020**, *220*, 121392.
- [12] M. Yuce, E. Filiztekin, K. G. Ozkaya, *Biosens. Bioelectron.* **2021**, *172*, 112752.
- [13] M. M. Bordbar, H. Samadinia, A. Hajian, A. Sheini, E. Safaei, J. Aboonajmi, F. Arduini, H. Sharghi, P. Hashemi, H. Khoshafar, M. Ghanei, H. Bagheri, *Sens. Actuators B Chem.* **2022**, *369*, 132379.
- [14] M. M. Bordbar, H. Samadinia, A. Sheini, J. Aboonajmi, M. Javid, H. Sharghi, M. Ghanei, H. Bagheri, *Microchim. Acta* **2022**, *189* (316), 1–11.
- [15] M. M. Bordbar, H. Samadinia, A. Sheini, J. Aboonajmi, H. Sharghi, P. Hashemi, H. Khoshafar, M. Ghanei, H. Bagheri, *Talanta* **2022**, *246*, 123537.
- [16] L. Lan, D. Xu, G. Ye, C. Xia, S. Wang, Y. Li, H. Xu, *Jama* **2020**, *323* (15), 1502–1503.
- [17] Y. Li, L. Yao, J. Li, L. Chen, Y. Song, Z. Cai, C. Yang, *J. Med. Virol.* **2020**, *92* (7), 903–908.
- [18] P. B. Van Kasteren, B. van der Veer, S. van den Brink, L. Wijsman, J. de Jonge, A. van den Brandt, R. Molenkamp, C. B. E. M. Reusken, A. Meijer, *J. Clin. Virol.* **2020**, *128*, 104412.
- [19] B. G. Andryukov, *AIMS Microbiol.* **2000**, *6* (3), 280–304.

- [20] E. Adams, M. Ainsworth, R. Anand, M. I. Andersson, K. Auckland, J. K. Baillie, E. Barnes, S. Beer, J. I. Bell, T. Berry, S. Bibi, M. Carroll, S.K. Chinnakannan, E. Clutterbuck, R. J. Cornall, D. W. Crook, T. de Silva, W. Dejnirattisai, K. E. Dingle, C. Dold, A. Espinosa, D. W. Eyre, H. Farmer, M. F. Mendoza, D. Georgiou, S. J. Hoosdally, A. Hunter, K. Jeffrey, P. Klenerman, J. Knight, C. Knowles, A. J. Kwok, U. Leuschner, R. Levin, C. Liu, C. López-Camacho, J. Martinez, P. C. Matthews, H. McGivern, A. J. Mentzer, J. Milton, J. Mongkolsapaya, S. C. Moore, M. S. Oliveira, F. Pereira, E. Perez, T. Peto, R. J. Ploeg, A. Pollard, T. Prince, D. J. Roberts, J. K. Rudkin, V. Sanchez, G. R. Sreaton, M. G. Semple, D. T. Skelly, E. N. Smith, A. Sobrinodiaz, J. Staves, D. I. Stuart, P. Supasa, T. Surik, H. Thraves, P. Tsang, L. Turtle, A. S. Walker, B. Wang, C. Washington, N. Watkins, J. Whitehouse, Antibody testing for COVID-19: A report from the National COVID Scientific Advisory Panel *medRxiv* **2020**, 1–21.
- [21] Y. Fang, H. Zhang, J. Xie, M. Lin, L. Ying, P. Pang, W. Ji, *Radiology* **2020**, *296* (2), E115–E117.
- [22] L. M. Kucirka, S. A. Lauer, O. Laeyendecker, D. Boon, J. Lessler, *Ann. Intern. Med.* **2020**, *173* (4), 262–267.
- [23] L. J. Carter, L. V. Garner, J. W. Smoot, Y. Li, Q. Zhou, C. J. Saveson, J. M. Sasso, A. C. Gregg, D. J. Soares, T. R. Beskud, S. R. Jervy, C. Liu, *ACS Cent. Sci.* **2020**, *6* (5), 591–605.
- [24] B. Udugama, P. Kadhiresan, H. N. Kozlowski, A. Malekjahani, M. Osborne, V. Y. C. Li, H. Chen, S. Mubareka, J. B. Gubbay, W. C. W. Chan, *ACS Nano* **2020**, *14* (4), 3822–3835.
- [25] A. Merkoçi, C.-Z. Li, L. M. Lechuga, A. Ozcan, *Biosens. Bioelectron.* **2021**, *178*, 113046.
- [26] R. Antiochia, *Microchim. Acta* **2020**, *187* (12), 639.
- [27] R. Antiochia, *Biosensors* **2021**, *11* (4), 110.
- [28] N. Karimian, P. Hashemi, A. Khanmohammadi, A. Afkhami, H. Bagheri, *Anal. Bioanal. Chem. Res.* **2020**, *7* (3), 281–301.
- [29] Z. Saberi, B. Rezaei, H. Faroukhpour, A. A. Ensafi, *Microchim. Acta* **2018**, *185* (303), 1–10.
- [30] H. Bagheri, E. Ranjbari, M. Amiri-Aref, A. Hajian, Y. H. Ardakani, S. Amidi, *Biosens. Bioelectron.* **2016**, *85*, 814–821.
- [31] S. Eissa, M. Zourob, *Anal. Chem.* **2021**, *93* (3), 1826–1833.
- [32] S. Eissa, H. A. Alhadrami, M. al-Mozaini, A. M. Hassan, M. Zourob, *Microchim. Acta* **2021**, *188*, 199.
- [33] L. Fabiani, M. Saroglia, G. Galatà, R. De Santis, S. Fillo, V. Luca, G. Faggioni, N. D'Amore, E. Regalbuto, P. Salvatori, G. Terova, D. Moscone, F. Lista, F. Arduini, *Biosens. Bioelectron.* **2021**, *171*, 112686.
- [34] R. M. Torrente-Rodríguez, H. Lukas, J. Tu, J. Min, Y. Yang, C. Xu, H. B. Rossiter, W. Gao, *Matter* **2020**, *3* (6), 1981–1998.
- [35] A. Yakoh, U. Pimpitak, S. Rengpipat, N. Hirankarn, O. Chailapakul, S. Chaiyo, *Biosens. Bioelectron.* **2021**, *176*, 112912.
- [36] Z. Rahmati, M. Roushani, *Microchim. Acta* **2022**, *189* (287), 1–10.
- [37] Z. Rahmati, M. Roushani, H. Hosseini, H. Choobin, *Bioelectrochemistry* **2022**, *146*, 108106.
- [38] Z. Rahmati, M. Roushani, H. Hosseini, H. Choobin, *Microchem. Journal* **2021**, *170*, 106718.
- [39] Z. Rahmati, M. Roushani, H. Hosseini, H. Choobin, *Microchim. Acta* **2021**, *188* (105), 1–9.
- [40] M. Alafeef, K. Dighe, P. Moitra, D. Pan, *ACS Nano* **2020**, *14* (12), 17028–17045.
- [41] G. Qiu, Z. Gai, Y. Tao, J. Schmitt, G. A. Kullak-Ublick, J. Wang, *ACS Nano* **2020**, *14* (5), 5268–5277.
- [42] G. Seo, G. Lee, M. J. Kim, S. H. Baek, M. Choi, K. B. Ku, C. S. Lee, S. Jun, D. Park, H. G. Kim, S. J. Kim, J. O. Lee, B. T. Kim, E. C. Park, S. I. Kim, *ACS Nano* **2020**, *14* (4), 5135–5142.
- [43] S. Yu, S. B. Nimse, J. Kim, K. S. Song, T. Kim, *Anal. Chem.* **2020**, *92*, 14139–14144.
- [44] M. Choudary, P. Yadav, A. Singh, S. Kaur, J. Ramirez-Vick, P. Chandra, K. Arora, S. P. Singh, *Electroanalysis* **2016**, *28* (10), 2565–2574.
- [45] I. T. Cavalcanti, M. I. F. Guedes, M. D. P. T. Sotomayor, H. Yamanakac, R. F. Dutraa, *Biochem. Eng. J.* **2012**, *67*, 2636–2639.
- [46] Y. T. Büyüksünetçi, B. E. Çitil, Ü. Anik, *Analyst* **2022**, *147*, 130.
- [47] H. A. Hussein, A. Kandeil, M. Goma, R. M. El Nashar, I. M. El-Sherbiny, R. Y. Hassan, *ACS Sens.* **2021**, *6*, 4098–4107.
- [48] M. D. T. Torres, W. R. de Araujo, L. F. de Lima, A. L. Ferreira, C. de la Fuente-Nunez, *Matter* **2021**, *4* (7), 2403–2416.
- [49] G. C. Zaccariotto, M. K. L. Silva, G. S. Rocha, I. Cesarino, *Materials* **2021**, *14*, 4230.
- [50] S. A. Hashemi, N. G. G. Behbahan, S. Baharani, S. M. Mousavi, A. Gholami, S. Ramakrishna, M. Firoozsani, M. Moghadami, K. B. Lankarani, N. Omidifar, *Biosens. Bioelectron.* **2021**, *171*, 112731.
- [51] L. Liv, G. Çoban, N. Nakiboglu, T. Kocagöz, *Biosens. Bioelectron.* **2021**, *192*, 113497.
- [52] B. Mojsoska, S. Larsen, D. A. Olsen, J. S. Madsen, I. Brandslund, F. A. Alatraktchi, *Sensors* **2021**, *21* (2), 390.
- [53] A. Raziq, A. Kidakova, R. Boroznjak, J. Reut, A. Öpik, V. Sviritski, *Biosens. Bioelectron.* **2021**, *178*, 113029.
- [54] H. Zhao, F. Liu, W. Xie, T. C. Zhou, J. OuYang, L. Jin, H. Li, C. Y. Zhao, L. Zhang, J. Wei, Y. P. Zhang, C. P. Li, *Sens. Act. B: Chem.* **2021**, *327*, 128899.
- [55] T. Chaiubun, J. Puenpa, T. Ngamdee, P. Boonapatcharoen, Athamanolap, A. P. O'Mullane, S. Vongpunsawad, Y. Poovorawan, S. Y. Lee, B. Lertanantawong, *Nat. Commun.* **2021**, *12* (1), 802.

Received: September 9, 2022
Accepted: September 15, 2022
Published online on ■■■, ■■■



*C. Tortolini, A. Angeloni, R. Antiochia**

1 – 11

A Comparative Study of Voltammetric vs Impedimetric Immunosensor for Rapid SARS-CoV-2 Detection at the Point-of-care

